



Obrabotka metallov -

Metal Working and Material Science

Journal homepage: http://journals.nstu.ru/obrabotka_metallov



Elastic modulus and hardness of Ti alloy obtained by wire-feed electron-beam additive manufacturing

Vasily Klimenov^{1, a*}, Evgeny Kolubaev^{2, b}, Zeli Han^{1, c}, Andrey Chumaevskii^{2, d}, Edgar Dvilis^{1, e}, Irina Strelkova^{1, f}, Ekaterina Drobyaz^{3, g}, Oleg Yaremenko^{4, h}, Aleksandr Kuranov^{4, i}

¹ National Research Tomsk Polytechnic University, 30 Lenin ave., Tomsk, 634050, Russian Federation

² Institute of Strength Physics and Materials Science of the Siberian Branch of the RAS, 2/4, pr. Akademicheskii, Tomsk, 634055, Russian Federation

³ Novosibirsk State Technical University, 20 Prospekt K. Marksa, Novosibirsk, 630073, Russian Federation

⁴ Opton Engineering Limited Liability Company Ugreshskaya str., 2, p. 53, Moscow, 115088, Russian Federation

^a  <https://orcid.org/0000-0001-7583-0170>,  klimenov@tpu.ru; ^b  <https://orcid.org/0000-0001-7288-3656>,  eak@ispm.s.tsc.ru;

^c  <https://orcid.org/0000-0001-6502-6541>,  hanzelizy@gmail.com; ^d  <https://orcid.org/0000-0002-1983-4385>,  tch7av@gmail.com;

^e  <https://orcid.org/0000-0002-6853-6448>,  dvilis@tpu.ru; ^f  <https://orcid.org/0000-0002-2222-2865>,  strelkova@tpu.ru;

^g  <https://orcid.org/0000-0002-5364-3574>,  ekaterina.drobyaz@yandex.ru; ^h  <https://orcid.org/0009-0002-8193-8027>,  oy@opton.ru;

ⁱ  <https://orcid.org/0009-0001-5593-9053>,  ak@opton.ru

ARTICLE INFO

Article history:

Received: 17 July 2023

Revised: 10 August 2023

Accepted: 18 September 2023

Available online: 15 December 2023

Keywords:

Wire-feed electron-beam additive manufacturing

Titanium alloys

Elastic modulus

Indentation

Ultrasonic control

Hardness

Funding

Research was supported by Grant No. 23-79-00066 from the Russian Science Foundation, <https://rscf.ru/project/23-79-00066/>.

Acknowledgements

The authors like to express their gratitude towards the management of the Academic Innovative Center of National Research Tomsk Polytechnic University for equipment employed in these studies, financially supported by the Ministry of Education and Science of the Russian Federation (Project No. 075-15-2021-710). These studies also employed equipment of the Core Facility Centre "Structure, Mechanical, and Physical Properties of Materials" of Novosibirsk State technical University. We thank S. Yu. Nikonov (Institute of Strength Physics and Materials Science SB RAS) for 3D printing of specimens.

ABSTRACT

Introduction. The development and application of additive manufacturing depends on many factors, including the printing process performance and buy-to-fly ratio. Wire-feed electron-beam additive manufacturing (*EBAM*) is attracting more and more attention from research teams. Moreover, the use of electron beams is the most effective and competitive for additive manufacturing of parts from alloys possessing high oxidation characteristics, e.g., titanium, stainless steels, since selective laser melting occurs in vacuum. Welding titanium wire *VT6sv* is the most preferable choice due to its availability and a wide range of thickness. This alloy, however, has fewer alloying elements than *VT6 (Ti-6Al-4V)* alloys. The high performance of wire-feed 3D printing and the *VT6sv* alloy composition affect the structure, phase composition, and properties of the fabricated alloy. As is known, the elastic modulus and hardness of alloys are important parameters, which can be measured rapidly also using non-destructive testing. **The purpose of this work** is to study the application of different approaches to measuring the elastic modulus and hardness of products obtained by wire-feed *EBAM* using the equipment of the *Institute of Strength Physics and Materials Science SB RAS*. **Research methods.** The structure of *VT6sv* titanium alloys fabricated by 3D printing and *VT1-0 (Grade 2)*, *VT6 (Ti-6Al-4V)* alloys, was investigated by different methods such as metallography, ultrasonic gauging, instrumented indentation technique, macro- and micro-indentation, indentation hardness testing. **Results and Discussion.** Titanium alloy fabricated from *VT6sv* titanium wire under different thermal conditions has a typical columnar structure throughout the forging height. The structure formation determines the elastic modulus and hardness at various points of the forging. It is found that the elastic modulus is higher than that of as-delivered *Ti-6Al-4V* alloys, while the hardness is lower. Micro-indentation shows lower values of the elastic modulus than macro-indentation, which approach to values obtained by ultrasonic gauging and in other works. Different values of the elastic modulus at different points of the 3D printed forging indicate its sensitivity to the structure and phase composition of the material and demonstrate capabilities of measuring techniques used in this work.

For citation: Klimenov V.A., Kolubaev E.A., Han Z, Chumaevskii A.V., Dvilis E.S., Strelkova I.L., Drobyaz E.A., Yaremenko O.B., Kuranov A.E. Elastic modulus and hardness of Ti alloy obtained by wire-feed electron-beam additive manufacturing. *Obrabotka metallov (tehnologiya, oborudovanie, instrumenty) = Metal Working and Material Science*, 2023, vol. 25, no. 4, pp. 180–201. DOI: 10.17212/1994-6309-2023-25.4-180-201. (In Russian).

* Corresponding author

Klimentov Vasily A., D.Sc. (Engineering), Professor
 National Research Tomsk Polytechnic University,
 30 Lenin ave.,
 634050, Tomsk, Russian Federation
 Tel.: +7 (3822) 701-777, e-mail: klimenov@tpu.ru

Introduction

Titanium (*Ti*) and titanium alloys are widely used in biomedicine due to its biocompatibility, corrosion resistance, and high specific strength. In the case with titanium prosthetic implants, its fatigue strength, tensile strength, and elongation are important in a substitution of load-bearing hard tissues [1]. Strength and hardness of parts fabricated by conventional techniques can be controlled rather easily, as its mechanical properties are almost the same as forgings it is obtained from. However, for example, when milling parts, some of materials go to waste. That is why additive manufacturing (*AM*) becomes more preferable both in medicine and other production activities based on expensive and hard-to-machine materials [2]. While, *AM* process parameters such as heat source power and velocity, surface power density, scanning mode, affect the melt pool shape and dimensions during the process. This determines the thermal cycle, cooling rate, temperature gradient, and solidification rate affecting the structure formation and properties of printed parts [3]. Mechanical properties of the material fabricated by selective laser melting (*SLM*) or directed energy deposition (*DED*), depending on the structure formation, determined by thermal conditions, are widely discussed by research teams. These studies are focused on the understanding of *AM* processes and its optimization [4–9], since the properties of fabricated products should satisfy standard requirements [10]. Both methods of material physics and mechanical strength testing accompanied by specimen disintegration are widely used. And interest in applying non-destructive testing, capable to detect and measure strength properties of the material, is understandable. Among mechanical properties that are most often measured by non-destructive testing methods, the elastic modulus and hardness, measured by ultrasonic testing [11–14], and elastic modulus, measured by instrumental indentation techniques [15–18], should be highlighted. When ultrasonic method is used to control the quality, the specimen retains its integrity. But the determination of the elastic modulus requires specific specimen geometry due to the structural performance and sensor dimensions. Only indentation techniques can therefore be really discussed as a prospect application of non-destructive testing method. A comparison of the elastic modulus, measured by indentation techniques and ultrasonic gauging, is very useful and informative [19]. Although *GOSTR 8.748-2011* gives the requirements for the macro- and micro-indentation loads, the obtained test results require thorough discussion and comparison [20].

It should be noted that elastic modulus is a key parameter in the material design and engineering. According to *Zolotarevsky* [21], the elastic modulus of pure metals is a low-sensitive parameter of the structure. In works [22, 23] it is found that this parameter changes during the transition of pure metals from coarse- to nano-crystalline state. Of great importance is the problem of the elastic modulus stability after different thermal treatment of *Ti* alloys, most of which consist of two phases [24]. According to numerous studies, elastic modulus, for example, for the *VT6 (Ti-6Al-4V)* alloy, ranges between 90 and 145 GPa [24]. It is shown that it depends on many factors, namely structure, its homogeneity, forging shape, and size of area to be measured.

Elastic modulus of *Ti* alloys used in medicine, is an important parameter, which determines biocompatibility of implants. Its reduction to the elastic modulus of bone tissue is gained by additional doping of alloys, which leads to significant changes in its structure and phase composition [25, 26]. Controlling the values of the elastic modulus of alloys, especially at the stage of technology development, is of great importance.

Ti alloys for additive manufacturing are exposed to a specific influence leading to the formation of inhomogeneous and anisotropic structures and phases. *SLM* or electron-beam additive manufacturing (*EBAM*) provide the formation of products with required properties [27]. The improvement of the economic efficiency of additive manufacturing, for example, increasing the wire-feed 3D printing performance, is associated with a complicated control for thermal conditions, and the alloy acquires a specific structure and phase composition [28, 29]. In the literature on *AM*-fabricated *Ti* alloys, information about the elastic modulus is obtained after processing tensile/compressive strain curves or after nanoindentation [29] and, to a lesser extent, after ultrasonic gauging [30]. In studying alloys with a complex structure and phase composition, it is expedient to apply several methods to measure the elastic modulus [31].

Today, the widespread instrumental indentation technique allows measuring the elastic modulus in real conditions, which also provides detection of other strength properties such as tensile strength, yield strength, crack resistance [32, 33].

This work presents studies on measuring the elastic modulus and hardness using ultrasonic gauging and macro- and micro-indentation of *VT6sv* titanium plates. The latter are fabricated by wire-feed *EBAM* and its properties are compared to those of *VT1-0*, *VT6* and *Ti-6Al-4V* alloys obtained by conventional techniques. Discussion of measurement results obtained for the elastic modulus and hardness by various techniques assists in further understanding of the obtained values on the structure and phase composition of *AM*-fabricated *Ti* alloys.

Methodology

Materials

In our experiments, the *Ti* alloy was fabricated by wire-feed *EBAM* using the welding titanium wire *VT6sv* with a diameter of 1.6 mm. The chemical composition of this wire met the requirements of *GOST 27265*. It differed from the *VT6* alloy in that the content of alloying elements corresponds to the lower limit of alloying values. Also, *VT1-0 (Grade 2)*, *VT6* and *Ti-6Al-4V* titanium rolled sheets were investigated. The chemical composition of *VT1-0* and *VT6* alloys matched *GOST 19807–91*, whereas the composition of the *Ti-6Al-4V* alloy corresponded to the China national standard *GB/T 3620.1-2016*. This is summarized in Table 1.

Table 1

Chemical composition of titanium alloys

Alloys	Ti	Al	V	Zr	Si	Fe	O	H	N	C	Impurities
<i>VT1-0 (Grade 2)*</i>	Base	–	–	–	0.10	0.25	0.20	0.010	0.04	0.07	0.10
<i>VT6*</i>	Base	5.3–6.8	3.5–5.3	0.30	0.10	0.60	0.20	0.015	0.05	0.10	0.30
<i>Ti-6Al-4V**</i>	Base	5.5–6.75	3.5–4.5	–	–	0.3	0.20	0.015	0.05	0.08	0.4
<i>VT6sv***</i>	Base	3.5–4.5	2.5–3.5	–	0.10	0.15	0.12	0.003	0.04	0.50	0.30

* *GOST 19807–91*

** *GB/T 3620.1-2016*

*** *GOST 27265–87*

Alloy specimens were fabricated on a laboratory *EBAM* system developed in the *Institute of Strength Physics and Materials Science SB RAS* [34]. The *EBAM* process was performed in vacuum, at a pressure ranging between 10^{-3} and 10^{-2} Pa. The $150 \times 60 \times 2.5$ mm³ titanium *VT1-0* substrate was positioned on a $160 \times 60 \times 5$ mm³ protective layer made of stainless steel. All this was mounted to a triaxial working table via metal clamps. The working table was equipped with liquid cooling, and during printing the temperature was maintained at 13–15 °C. After the 20th layer, the beam current was reduced from 55 to 40 mA to decrease the heat input. *CAD*-assisted 3D printing provided the fabrication of $100 \times 60 \times 8$ mm³ plate, one plate is demonstrated in Fig. 1, *a*. The obtained plates were milled and polished for ultrasonic gauging, indentation, and hardness measurement in $89 \times 39 \times 3$ mm³ areas indicated in Fig. 1, *b*.

Ultrasonic gauging

In order to detect the elastic modulus and hardness by ultrasonic gauging, instrumental indentation and metallography, the electric discharge machining was used for cutting test specimens from different sectors of the plate. Cutting was performed according to the requirements for specimen dimensions in these measuring techniques.

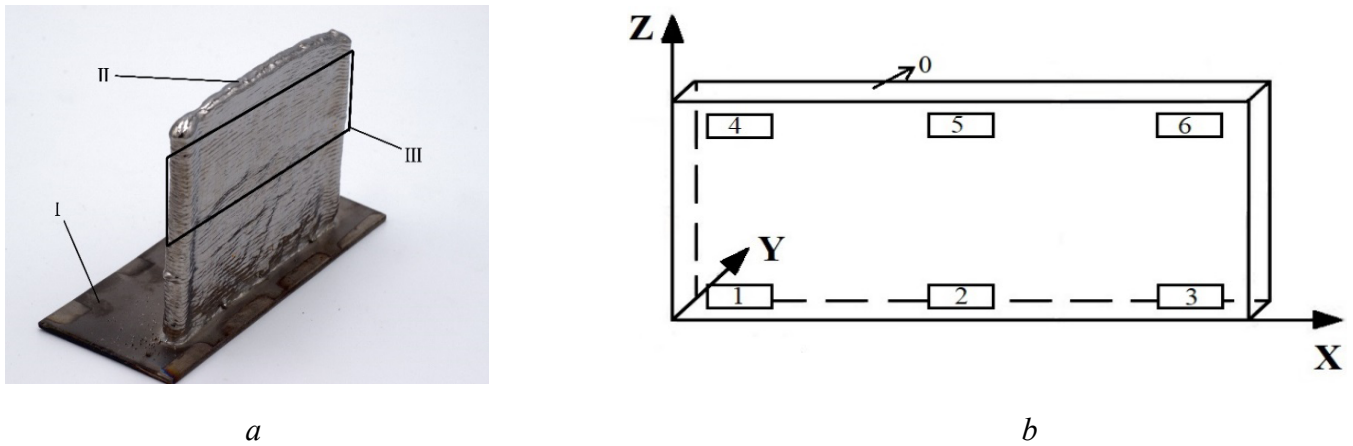


Fig. 1. General view of 3D printed specimen (a): I – VTI-0 substrate, II – wire-feed EBAM plate, III – cut area for testing; indentation measurement segments (b): 0 – in XY plane, 1 – 6 – in XZ plane

The ultrasonic thickness gauge 38DL PLUS (Olympus), presented in Fig. 2, a, was used to measure the elastic modulus. The requirements for the specimen dimensions were determined by the size of the shear wave probe V156 (5 MHz) and longitudinal wave probe V112 (10 MHz). The specimen height should exceed the probe diameter (Fig. 2, b).

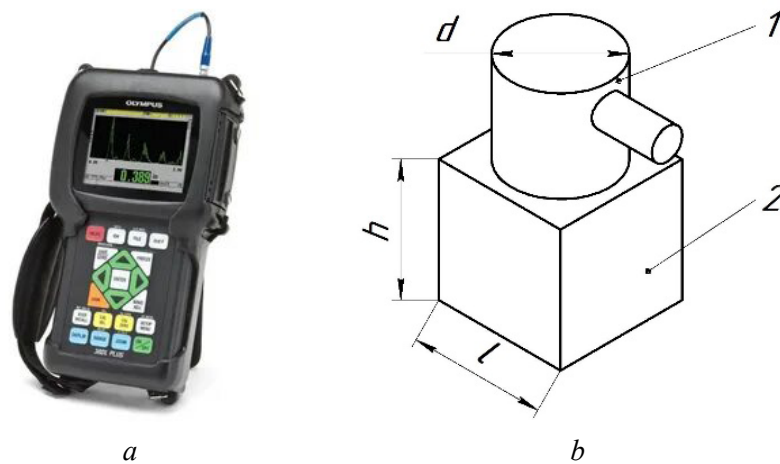


Fig. 2. Photograph of ultrasonic thickness gauge 38DL PLUS (a); schematic ultrasonic gauging (b): 1 – probe, 2 – specimen

The mean thickness value was obtained after 10 measurements of each specimen. The wave velocity was obtained by measuring the specimen thickness and the time of the wave propagation. Poisson's ratio ν and elastic modulus E were calculated from (1) and (2):

$$\nu = \frac{1 - 2(V_T / V_L)^2}{2 - 2(V_T / V_L)^2}; \quad (1)$$

$$E = \frac{V_L^2 \rho (1 + \nu)(1 - 2\nu)}{1 - \nu}, \quad (2)$$

where V_T is the shear acoustic velocity; V_L is the longitudinal acoustic velocity equaling the doubled thickness divided by the time of back and forth propagation; ρ is the density.

The elastic modulus was calculated according to ASTM E494-15 [35].

Indentation elastic modulus

Macro-indentation

Measurement of the elastic modulus during macro-indentation of a *Ti* alloy plate fabricated by 3D printing was carried out by the instrumental indentation system *AIS3000 HD* (*FRONTICS*, Korea) [32, 33, 36] presented in fig. 3, *a*, *b*. The procedure is schematically illustrated in fig. 3, *c*, *d*.

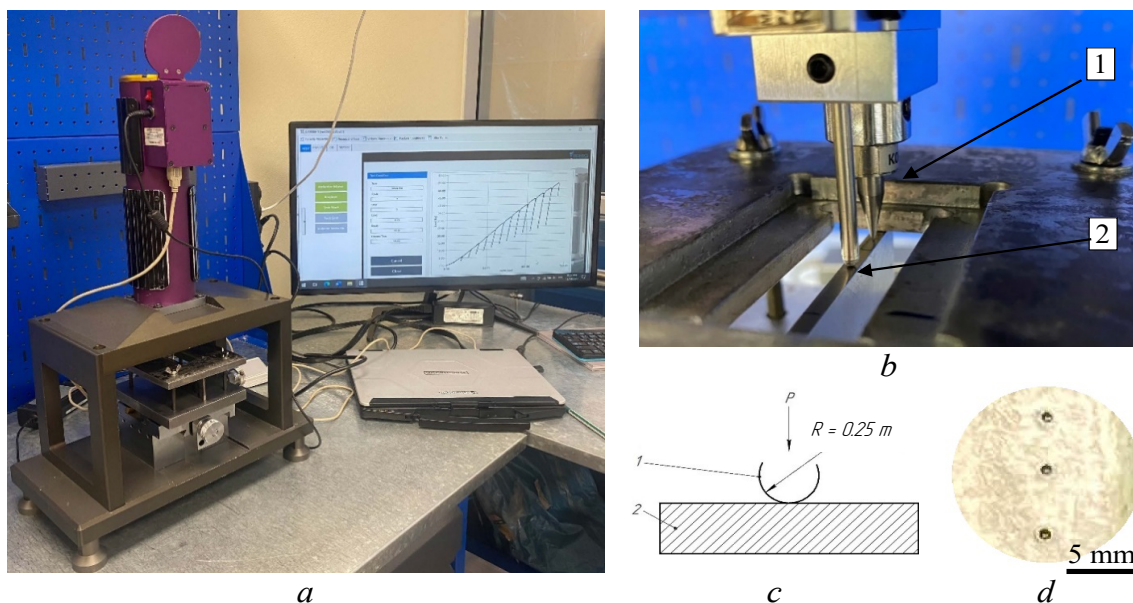


Fig. 3. General view of the *AIS3000 HD* (*a*); indentation assembly (*b*):

1 – *Vickers* indenter (Dia. 0.5/1.0 mm), 2 – specimen; schematic indentation (*c*): 1 – rounded tip, 2 – specimen; points of indentation (*d*)

The *AIS3000 HD* operating principle is based on the penetration of an indenter into the inspected object under a gradual loading and subsequent periodic partial unloading followed by complete unloading after reaching the maximum penetration depth. Firmware controls the system operation and displays control parameters such as load, depth, loading rate. External software is installed on a *PC* to control the system operation and display, store, communicate, and statistically process results of measurement. External software detects such properties as elastic modulus, hardness, residual stress, tensile strength, and crack resistance (fracture toughness) based on the load-penetration curve.

The indentation load is measured by a strain gauge, and the indentation depth is determined by a displacement sensor. The system operation is based on instrumented indentation, i.e., indentation of the tip (indenter) into the inspected material according to both *GOST R 8.748-2011* [17] and *ASTM E2546-15* [15]. The instrumental indentation technique helps to determine the dependence between the penetration force and depth at its gradual variation. The *AIS3000 HD* provides fast and easy inspection not only of parts, but also various products.

A *WC* spherical indenter with a radius of 250 μm was used for indentation at a load of 600 N. Each test included 15 “loading \rightarrow partial loading \rightarrow intermittent unloading” cycles at a loading rate of 0.3 mm/min. Load-penetration curves were continuously obtained during indentation and then converted into “true stress-true strain” curves. All indentation tests were performed at room temperature.

The elastic modulus is determined by the contact stiffness S (the slope of the tangent to the unloading curve when the force F is removed, shown in fig. 4). The straight section of the unloading curve describes the elastic recovery of the material. The unloading curve can be expressed as:

$$F = k(h - h_f)^m, \quad (3)$$

where m and k are correlation constants.

$$S = \left(\frac{dF}{dH} \right)_{h=h_{\max}} = km(h_{\max} - h_f)^{m-1} = \frac{2}{\sqrt{\pi}} E_r \sqrt{A_c}, \quad (4)$$

$$\frac{1}{E_r} = \frac{1 - \nu^2}{E} + \frac{1 - \nu_i^2}{E_i}, \quad (5)$$

where ν and ν_i are *Poisson's ratios* for the material and indenter, respectively; E_r is the reduced elastic modulus; E_i is the elastic modulus of the indenter tip.

The equation that describes the reduced elastic modulus is as follows:

$$E_r = \frac{\sqrt{\pi}}{2} S \frac{1}{\sqrt{A_c}}, \quad (6)$$

where A_c is the actual contact area of the spherical indenter tip with regard to the height of the plastic pile-up h_{pile} and the elastic contact depth h_e .

The real contact area A_c is determined with respect to the actual contact radius a and is the function h_c of the contact depth and the material:

$$A_c = f(h_c). \quad (7)$$

The contact depth at the current penetration force can be obtained from the analysis of the unloading curve (fig. 4) using the indenter geometry, elastic strain, and morphology of deformed surface.

In figs. 4 and 5, the following notations are used:

F_{\max} : Maximum penetration force;

h_p : Residual indentation depth after F_{\max} removal from the specimen;

h_i : Point of intersection of the tangent to curve at F_{\max} with the indentation depth-axis;

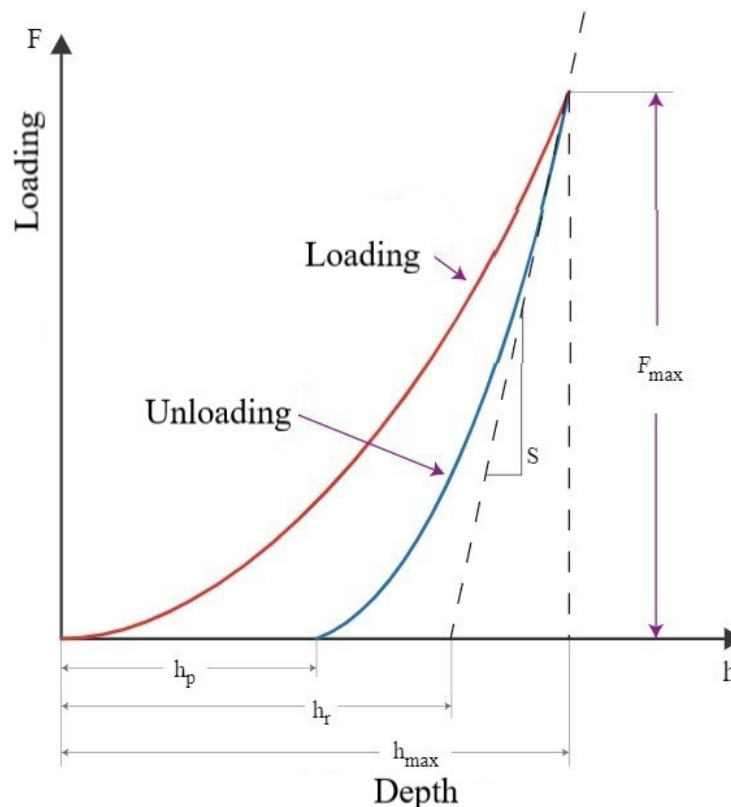


Fig. 4. Schematic “loading/unloading” curves of indentation for a single cycle

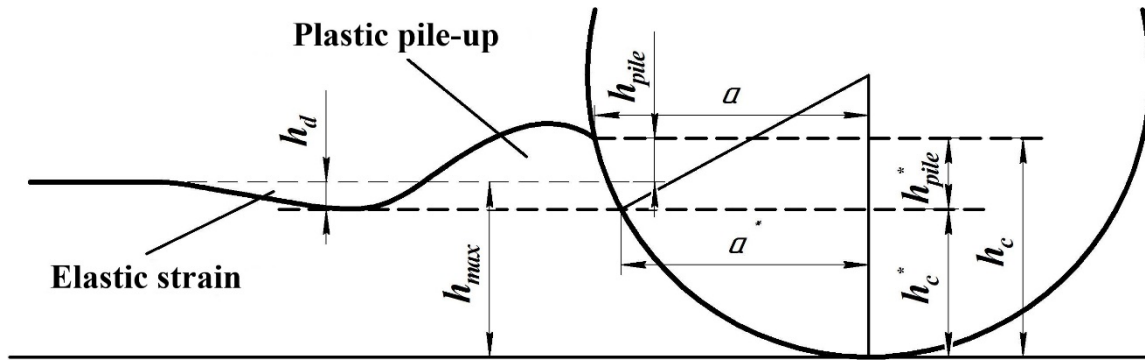


Fig. 5. Morphology of deformed surface of the material

- h_{max} : Maximum indentation depth at F_{max} ;
 - h_c : Depth of the contact of the indenter with the test piece at F_{max} ;
 - h_{pile}^* : Height of plastic pile-up;
 - h_d : Depth of elastic contact;
 - R : Radius of spherical tip;
 - a : Actual contact radius;
 - a^* : Contact radius without pile-up.
- We thus obtain:

$$h_c = h_c^* + h_{pile}^* = h_{max} - h_d + h_{pile}^* \tag{8}$$

$$h_d = \omega(h_{max} - h_r) = 0,75F_{max} / S, \tag{9}$$

where ω is the indenter shape index equaling 0.75 for spherical tip.

Therefore,

$$h_c^* + h_{pile}^* = h_{max} - (0,75F_{max} / S) + h_{pile}^*, \tag{10}$$

$$\frac{h_{pile}^*}{h_c^*} = f\left(n_{IT}, \frac{h_{max}}{R}\right). \tag{11}$$

The plastic pile-up can be expressed through the constant c and connected with the strain hardening n of the material by the empirical relation

$$c^2 = \frac{a^2}{a^{*2}} = \frac{5(2-n)}{2(4+n)}, \tag{12}$$

where a is the actual contact radius; a^* is the contact radius without pile-up.

Based on the geometry of the spherical indenter, the actual contact radius is expressed as h_c and the indenter radius R :

$$a^2 = \frac{5(2-n)}{2(4+n)}(2Rh_c^* - h_c^{*2}). \tag{13}$$

The actual contact area A_c is determined by the actual contact depth h_c correlating with h_{pile}^* and h_c^* :

$$A_c = \pi(2Rh_c - h_c^2). \tag{14}$$

Micro-indentation

The elastic modulus and microhardness testing was performed on a *DUH-211S* Dynamic Ultra Microhardness Tester (*Shimadzu*, Japan) fitted with a *Berkovich* three-sided pyramid indenter with $\alpha = 65.03^\circ$. The maximum test force was 2,000 mN (fig. 6).

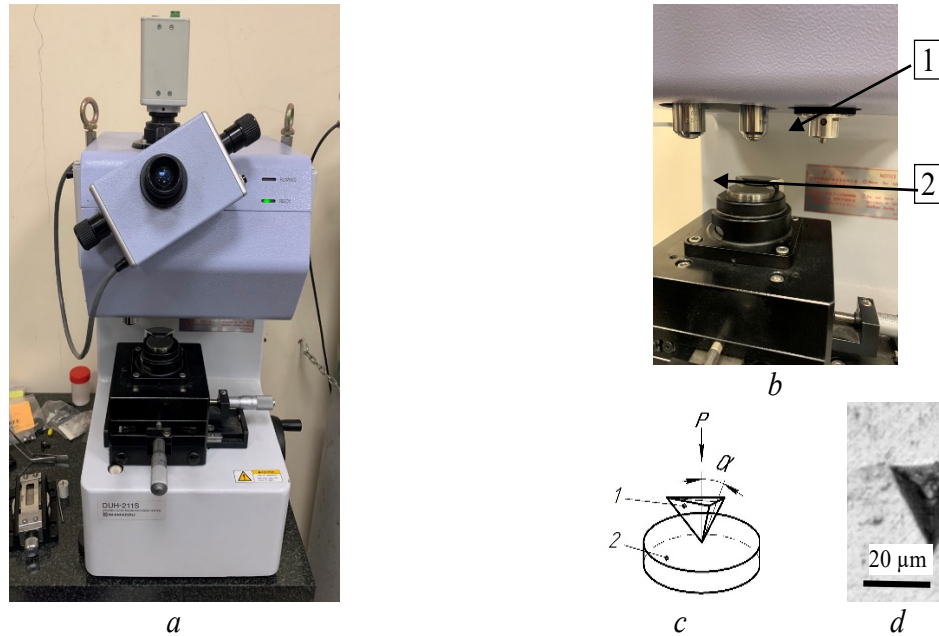


Fig. 6. General view of a *DUH-211S* Dynamic Ultra Microhardness Tester (a); test section (b); 1 – probe, 2 – specimen; schematic loading (c): 1 – *Berkovich* indenter, 2 – specimen; point of indentation (d)

The indentation elastic modulus is calculated from (5), where *Poisson's* ratio for diamond is 0.07, the elastic modulus for diamond is $1.14 \cdot 10^6$ N/mm², in this case the reduced elastic modulus in the indentation region E_r is determined as follows:

$$E_r = \frac{S\sqrt{\pi}}{2\sqrt{A_p}}, \quad (15)$$

where A_p is the cross-sectional area of the contact surface between the tip and specimen, which is determined by the load curve on $F-h$ diagram and the tip area function.

For the *Berkovich* tip, A_p is calculated as follows:

$$\sqrt{A_p} = 4.896h_c. \quad (16)$$

The *DUH-211S* provides a continuous measurement of the material stiffness along with loading and displacement as a continuous function of the penetration depth. The hardness and elastic modulus are calculated at each data point recorded during testing.

Microhardness measurement

A *DuraScan-10* hardness tester (*EMCO-TEST*, Austria) for high load range testing was used to measure the hardness under 100 g load for 3 s. Measurement was conducted in the XZ plane, on the left side at point θ (see fig. 1, b).

Metallography and elemental analysis

The preparation of specimens for metallographic studies and elemental analysis was carried out by cutting it from various sections of the printed plate and then grinding the surfaces using sandpaper with a consistently decreasing grain size of the abrasive. Final polishing was carried out using diamond paste.

The microstructure of the specimens was investigated using an *Axio Observer A1m* Inverted Microscope (*Carl Zeiss*, Germany) after chemical etching with *Kroll's* reagent consisting of 10 mL HNO_3 , 3 mL HF , and 87 mL H_2O .

An Oxford Instruments *INCA X-Act* Energy dispersive X-ray (*EDX*) spectroscopy on the scanning electron microscope *Zeiss EVO 50 XVP* (Germany) was carried out to investigate the fine structure and chemical composition of the structural elements. The *EDX* analysis was performed in two planes with a scanning step of 0.25 μm .

Results and discussion

Structure and elemental composition

Materials fabricated by selective laser melting (*SLM*) or wire-feed *EBAM* are characterized by the heterogeneous and anisotropic structure and properties [28], determined by layer-by-layer fusing by the electron beam. It is well known that cooling rates in the majority of conventional casting techniques can range from several tens to a thousand of kelvin per second, which induces significant changes in the structure and properties of the manufactured material. In additive manufacturing, cooling rates of the melt can range from 10^3 to 10^8 K/s. Moreover, temperature gradients reach 10^6 K/cm [37] in some regions. The structural features and its effects on the properties of titanium alloys were most often evaluated using metallography methods and mechanical tests for hardness and strength, mainly under tension, for specimens obtained by selective laser melting [38, 39]. In wire-feed *EBAM*, when the layer thickness is considerably higher than in *SLM*, temperature conditions conform with lower cooling rates, that is proven by the columnar structure, presented in fig. 7, *a*, and the cross-section of columnar crystals in the form of polygons with diagonals of

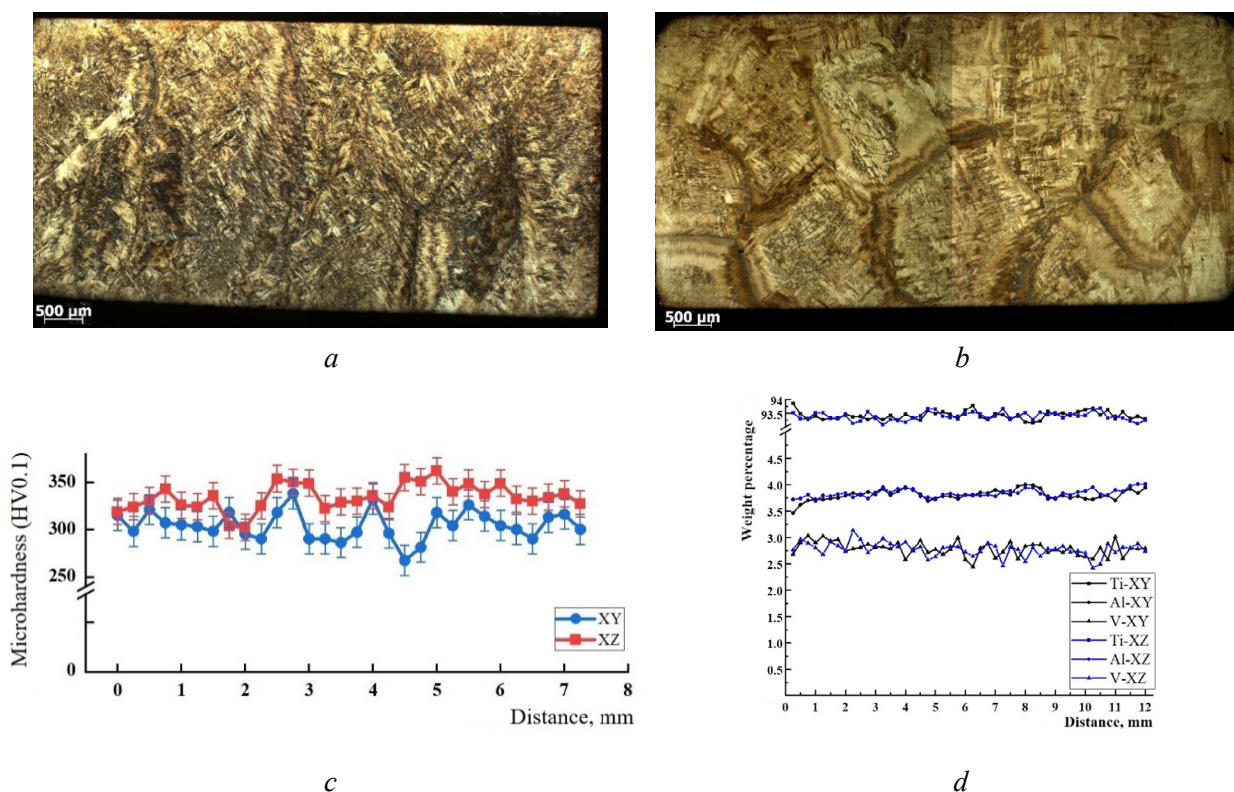


Fig. 7. SEM images with *EDX* analysis in *XZ* (a) and *XY* (b) planes; microhardness distribution (c); elemental analysis (d)

1 to 2.0 mm in the beam scanning plane, as shown in fig. 7, *b*. The nature of the change in microhardness values in the presented planes also indicates structural inhomogeneities in the forming grains (fig. 7, *c*).

The average microhardness values calculated for *XZ* and *XY* planes differ from each other, viz. 334 ± 14 HV0.1 and 304 ± 16 HV0.1, respectively. Unlike the *EDX* analysis of the microhardness distribution, the *EDX* analysis of the elemental distribution in weight percentage (fig. 7, *d*) at different points shows no significant change, which indicates the leading role of inhomogeneity of the structure, rather than the phase.

Ultrasonic gauging of elastic modulus and Poisson's ratio

The elastic modulus and *Poisson's* ratio for specimens prepared from different alloys are presented in table 2.

Table 2

Elastic properties determined by the 38DL PLUS

Alloys → Properties ↓	<i>VT1-0</i> *	<i>VT6</i> *	<i>Ti-6Al-4V</i> *	3D printed <i>VT6sv</i>
Elastic modulus <i>E</i> , GPa	109±1	120±1	130±1	131±1
<i>Poisson's</i> ratio, ν	0.33±0.03	0.32±0.03	0.31±0.03	0.27±0.03

* As-rolled alloys

As reported in early research [40] on the values of elastic moduli of commercially pure *Ti* alloy and *Al*- and *V*-doped *Ti* alloys, this parameter for cast alloys was 92 and 108 GPa at 160 and 294 HV, respectively. At the same time, the sensitivity of the elastic modulus to the phase composition and crystal structure was observed. The structure formation and properties of such alloys were investigated in [34, 41]. The structure consisted of lamellas and $\alpha + \beta$ phase colonies of different length and width. β -phase lamellas were smaller and located between α -phase lamellas, as presented in fig. 7a, b. It is very important that the presence of the β -phase provided its hardness growth even in the presence of the martensitic α' -phase. That indicated the predominant role of the solid solution hardening. The elastic modulus decreased with increasing content of the β -phase [42]. It was important to compare the data of titanium master alloys and commercially pure titanium, since the latter possessed a homogeneous structure unlike binary master alloys [43].

According to reference data in recent research, the elastic modulus is 100 to 110 GPa for pure titanium and *Ti-6Al-4V* system alloys, either cast or rolled [43] and 120 to 125 GPa at 400 to 420 HV hardness of the master alloy, respectively [27]. At the same time, the elastic modulus measured by ultrasonic gauging is 120 GPa for pure titanium in the initial state [43].

As can be seen from table 2, the elastic modulus for *VT1-0* and *VT6* alloys is in good agreement with that obtained in [27, 43], whereas the elastic modulus for the *Ti-6Al-4V* alloy significantly differs due to, probably, significant difference in its structure and phase composition.

Instrumental indentation [19, 22, 33, 36, 43] and nanoindentation [27] measurements of the elastic modulus for *Ti* alloys obtained by both conventional methods and additive manufacturing, are more common than ultrasonic gauging [19, 43].

Macro-indentation of elastic modulus and microhardness

The macro-indentation depth is ~ 150 μm , indentation point diameter is 0.5 mm (fig. 3d), which does not violate the integrity of the sample material and does not change its physical properties. At the same time, the dimensions of the material involved in the measurements exceed those analyzed during nanoindentation by more than an order of magnitude and are commensurate with the grain sizes. The elastic modulus is detected using the load-unload curves obtained by the above-described procedure and presented in fig. 8. The indenter penetration in the material induces its stress-strain state.

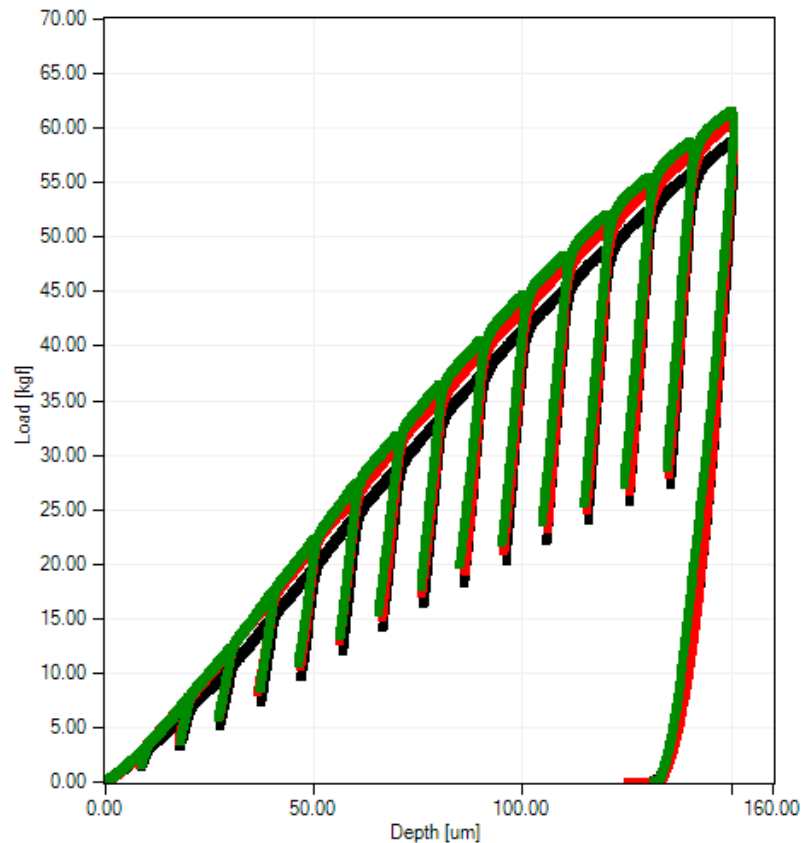


Fig. 8. Load-penetration curves of instrumental indentation using the AIS3000 HD

Indentation with multiple intermittent unloading results in a set of parameters in a wide indentation range, i.e., at different depth of penetration with gradually increasing penetration force. Using these parameters, the reduced elastic modulus is calculated in the whole range of elastoplastic deformation in the indentation zone. The elastic modulus and microhardness, obtained in XZ and XY planes, are shown in fig. 9.

As can be seen in fig. 9, a , b , absolute hardness values at different points with the structure shown in fig. 7, a , differ insignificantly, while in-plane hardness values matching structures shown in fig. 7, b , are slightly lower. Similar findings are presented in many works. As for absolute values of the elastic modulus, it differs from each other at different points and planes. As in the case with rolled alloys, the elastic modulus is different in the scanning plane and growth plane (fig. 9, b , c). And its absolute values are considerably lower than those obtained by ultrasonic testing.

Micro-indentation of elastic modulus and hardness

Load-depth curves in fig. 10 are obtained for four alloys. Great difference in the residual penetration depth indicates different resistance to deformation or hardness of alloys. One can see that after unloading, the residual depth for the $VT1-0$ alloy is higher than for other alloys. It means that this alloy is softer, while for other alloys, the tangent slope is close to the unloading curve.

Table 3 presents the elastic modulus and hardness for Ti alloys measured by various indentation techniques in different planes.

In this table, terms *longitudinal* and *vertical* mean that the indentation load is applied in XZ and XY rolling planes, respectively.

The obtained hardness values correspond to the values inherent in the alloys under study and show a difference depending on the measurement plane, both for rolled material $VT1-0$ and printed $VT6cv$. Values of the elastic modulus demonstrate its dependence on the structure and phase composition of Ti alloys. According to *Lutfullin et al.* [24], in Ti alloys consisting of a hexagonal α -phase and body centered cubic

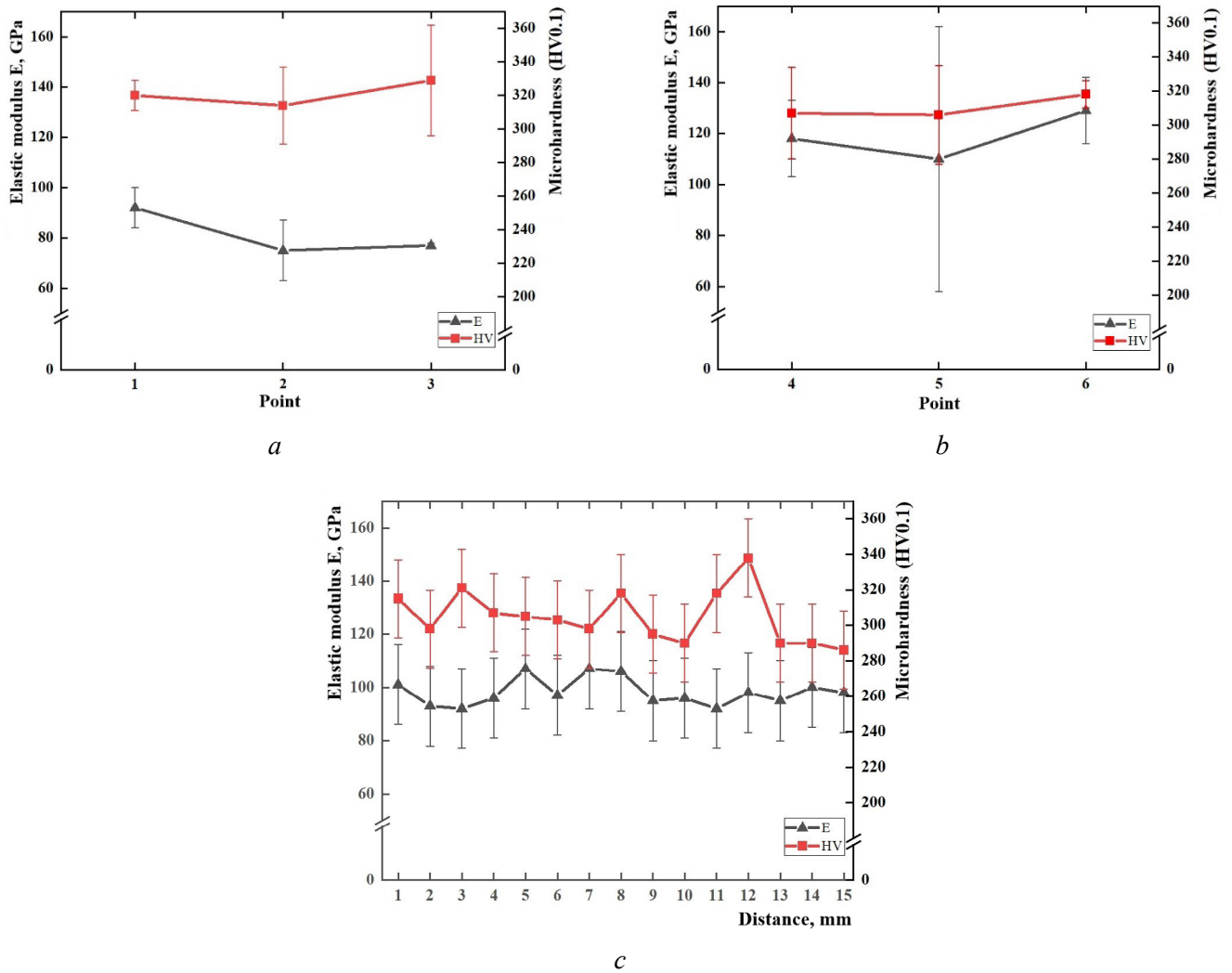


Fig. 9. Elastic modulus and hardness measured by the AIS3000 HD at different points: a – points 1, 2, 3; b – points 4, 5, 6; c – point 0 (XY plane)

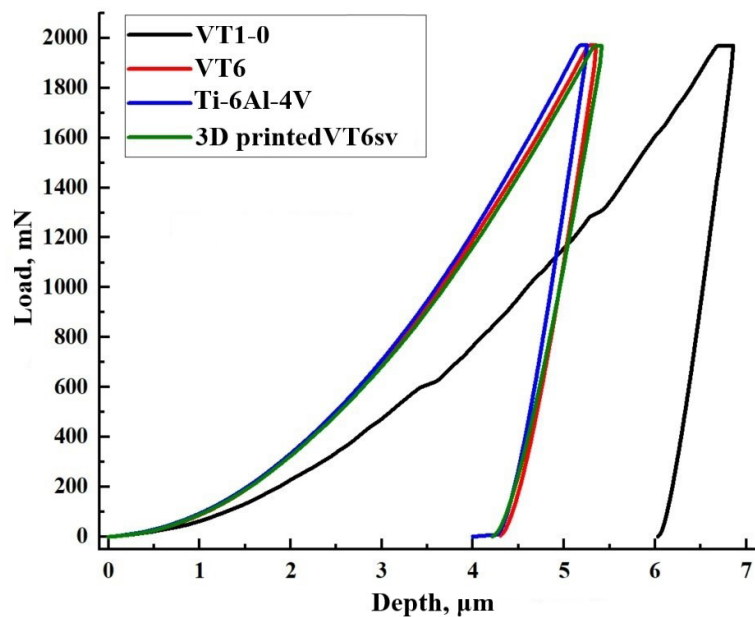


Fig. 10. Load-depth curves

Physical and mechanical properties of *Ti* alloys

Alloys → / Measurement methods and properties ↓		<i>VTI-0</i> *		<i>Ti-6Al-4V</i> *	3D printed <i>VT6sv</i>		<i>VT6</i> *	
Macro-indentation		E , GPa	Longitudinal	110±8	110±13	<i>XZ</i>	103–131	108±4
			Vertical	102±3	111±10	<i>XY</i>	90–100	
Micro-indentation	<i>DuraScan-10</i>	HV0.1	Longitudinal	168±5	370±23	<i>XZ</i>	334±14	339±6
			Vertical	170±6	375±25	<i>XY</i>	304±16	
	<i>DUH-211S</i>	E_{IT} = 0.5 GPa	99±3		94±1	90–100		90±2
		H_{IT} = 0.5 N/mm ²	1930±152		3913±129	3552±259		3660±105

Note. E_{IT} : Indentation elastic modulus, H_{IT} : Indentation hardness

*As-rolled alloys

β -phase (*VT6*, *Ti-6Al-4V* and *VT6sv*), the elastic modulus may depend on the ratio between these phases, as the elastic modulus for the α -phase is higher than for the β -phase. *Lutfullin et al.* attribute changes in the elastic modulus not only to the structure and phase composition of the 3D-printed *VT6sv* alloy, but also to the crystallographic texture. The latter plays an important role for the single-phase *VTI-0* alloy. As reported in [43], this alloy predictably manifests a homogeneous structure and is often used as a standard material for nanoindentation measurements of the elastic modulus for *Ti* alloys. As for the welding titanium wire *VT6sv* subjected to remelting and thermal treatment during 3D printing, we observe changes in its structure and phase composition (see fig. 7). In addition, phases and texture modified by temperature conditions in different parts of the specimen, also affect the elastic modulus [34]. It should be noted that temperatures below the β -transus temperature, induce the formation of several structural types in the *SLM Ti-6Al-4V* alloy, namely: allomorphic crude lamellas, small lamellas/aciculae, and α -phase grains [44]. The formation of these structures can be observed in *SLM* titanium alloys [27, 30]. Structural elements include a finer grain structure and martensite. The grain size and martensitic component depend on the 3D printing mode, which determines the hardness and elastic modulus of the product. Its hardness significantly exceeds that of the product fabricated from the rolled alloy, i.e., 5 or 6 and 3 or 4 GPa, respectively. As for the elastic modulus, it is slightly lower than that of the product fabricated from cast or rolled *Ti* alloys, i.e., 107 to 119 GPa and 110 to 125 GPa, respectively. In wire-feed *EBAM*, the layer thickness is much higher than in *SLM* forgings, and temperature conditions approach to those of casting. In wire-feed *EBAM*, the well-defined columnar structure appears throughout the forging height and equiaxial grain structure in the scanning plane (see fig. 7, *a, b*). Such an alloy structure provides its hardness common to cast alloys, which slightly differs from the hardness in planes of forming and scanning.

The elastic modulus obtained for all specimens, is much lower than that measured by ultrasonic gauging (see table 2). The highest difference in its values is conditioned by micro-indentation. The same difference is observed in [43], where the elastic modulus is measured by ultrasonic gauging and nanoindentation; besides the attention was drawn to the fact that the accuracy should be expected to be higher if the indentation covers a larger volume.

All findings of the elastic modulus and hardness for the *VT6sv* alloy fabricated by wire-feed *EBAM* and *Ti-6Al-4V* and *VT6* alloys in various states are presented in fig. 11, *a*. According to this figure, the elastic modulus obtained by ultrasonic testing for the printed material and rolled *Ti-6Al-4V* alloy, is slightly higher than that of initial cast and rolled alloys and those fabricated by *EB-PBF* in other works. Micro-indentation of the elastic modulus shows lower values than macro-indentation and findings of other researchers. Notably, the hardness of specimens printed from the *VT6sv* wire is lower than that of the *Ti-6Al-4V* alloy. This is explained by the *VT6sv* alloy composition, structure (see fig. 7), and microstructure [34]. The data presented in fig. 11, *b* correspond to cast alloys.

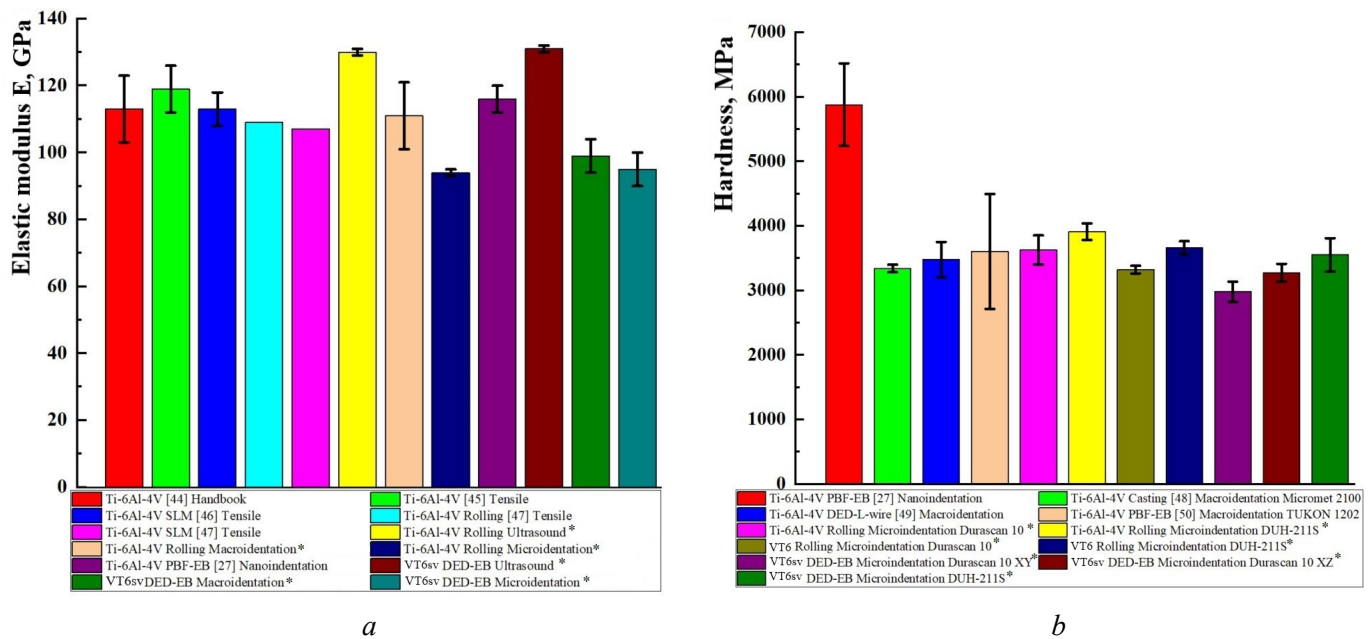


Fig. 11. Elastic modulus (a) and hardness (b) for *Ti* alloys. Abbreviations:

SLM – selective laser melting; *EB-DED* – electron beam directed energy deposition; *EB-PBF* – electron beam powder bed fusion; *L-DED* – laser directed energy deposition. Values obtained in this work are marked with an asterisk*

Conclusions

1. Elastic modulus and hardness are obtained for the *Ti* alloy fabricated by wire-feed *EBAM* with use of the *VT6sv* wire. These parameters were measured by using three techniques: ultrasonic gauging, macro-, and micro-indentations. The obtained values are compared to those obtained for different rolled *Ti* alloys and those described in other works.

2. The elastic modulus of *Ti* alloys with different structure and phase composition are in range of 90–100 GPa (macro-indentation) and 103–131 GPa (macro-indentation). These values correspond to the values for the initial and *EBAM*-fabricated alloys.

3. The elastic modulus for the alloy fabricated by wire-feed *EBAM*, are slightly higher than the known values presented in the literature, namely 131 and 125 GPa, respectively. On the contrary, the hardness is lower and matches the hardness of respective cast alloys.

4. Micro-indentation of the elastic modulus shows lower values than that when using macro-indentation; it is close to the elastic modulus obtained by ultrasonic gauging and in other works.

5. The difference between values of the elastic modulus at various points of the forging indicates its sensitivity to the structure and phase composition and demonstrated capabilities of described measurement techniques.

References

- Niinomi M. Mechanical properties of biomedical titanium alloys. *Materials Science and Engineering: A*, 1998, vol. 243 (1–2), pp. 231–236. DOI: 10.1016/s0921-5093(97)00806-x.
- Milewski J.O. *Additive manufacturing of metals: from fundamental technology to rocket nozzles, medical implants, and custom jewelry*. Cham, Springer, 2017. 343 p. ISBN 3319863487. DOI: 10.1007/978-3-319-58205-4.
- DebRoy T., Mukherjee T., Wei H.L., Elmer J.W., Milewski J.O. Metallurgy, mechanistic models and machine learning in metal printing. *Nature Reviews Materials*, 2021, vol. 6 (1), pp. 48–68. DOI: 10.1038/s41578-020-00236-1.
- Murr L.E., Gaytan S.M., Ramirez D.A., Martinez E., Hernandez J., Amato K.N., Shindo P.W., Medina F.R., Wicker R.B. Metal fabrication by additive manufacturing using laser and electron beam melting technologies. *Journal of Materials Science and Technology*, 2012, vol. 28 (1), pp. 1–14. DOI: 10.1016/S1005-0302(12)60016-4.



5. Murr L.E., Esquivel E.V., Quinones S.A., Gaytan S.M., Lopez M.I., Martinez E.Y., Medina F., Hernandez D.H., Martinez E., Martinez J.L., Stafford S.W., Brown D.K., Hoppe T., Meyers W., Lindhe U., Wicker R.B. Microstructures and mechanical properties of electron beam-rapid manufactured Ti-6Al-4V biomedical prototypes compared to wrought Ti-6Al-4V. *Materials Characterization*, 2009, vol. 60 (2), pp. 96–105. DOI: 10.1016/j.matchar.2008.07.006.
6. Facchini L., Magalini E., Robotti P., Molinari A. Microstructure and mechanical properties of Ti-6Al-4V produced by electron beam melting of pre-alloyed powder. *Rapid Prototyping Journal*, 2009, vol. 15 (3), pp. 171–178. DOI: 10.1108/13552540910960262.
7. Gong X., Lydon J., Cooper K., Chou K. Beam speed effects on Ti-6Al-4V microstructures in electron beam additive manufacturing. *Journal of Materials Research*, 2014, vol. 29 (17), pp. 1951–1959. DOI: 10.1557/jmr.2014.125.
8. Pushilina N., Stepanova E., Stepanov A., Syrtanov M. Surface modification of the EBM Ti-6Al-4V alloy by pulsed ion beam. *Metals*, 2021, vol. 11 (3), p. 512. DOI: 10.3390/met11030512.
9. Fedorov V.V., Rygin A.V., Klimenov V.A., Martyushev N.V., Klopotov A.A., Strelkova I.L., Matrenin S.V., Batranin A.V., Deryusheva V.N. Strukturnye i mekhanicheskie svoistva nerzhavayushchei stali, sformirovannoi v usloviyakh posloinogo splavleniya provoloki elektronnyim luchom [Structural and mechanical properties of stainless steel formed under conditions of layer-by-layer fusion of a wire by an electron beam]. *Obrabotka metallov (tekhnologiya, oborudovanie, instrumenty) = Metal Working and Material Science*, 2021, vol. 23, no. 4, pp. 111–124. DOI: 10.17212/1994-6309-2021-23.4-111-124.
10. Suo H., Chen Z., Liu J., Gong S., Xiao J. Microstructure and mechanical properties of Ti-6Al-4V by electron beam rapid manufacturing. *Rare Metal Materials and Engineering*, 2014, vol. 43 (4), pp. 780–785. DOI: 10.1016/s1875-5372(14)60083-7.
11. ASTM D2845-08. *Standard test method for laboratory determination of pulse velocities and ultrasonic elastic constants of rock* (Withdrawn 2017). ASTM International, 2008.
12. GB/T 38897-2020. *Non-destructive testing – Measurement method for material elastic modulus and Poisson's ratio using ultrasonic velocity*. State Administration for Market Regulation, National Standardization Administration. China, 2020. 20 p. (In Chinese).
13. State Standard 25095–82. *Sintered hardmetals. Method of determination of elastic modulus (of Young's modulus)*. Moscow, Standards Publ., 1982. 10 p. (In Russian).
14. GOST R 57862–2017. *Composites. Determination of dynamic young's modulus, shear modulus and Poisson's ratio by sonic resonance*. Moscow, Standartinform Publ., 2017. 15 p. (In Russian).
15. ASTM E2546-15. *Standard practice for instrumented indentation testing*. ASTM International, 2015.
16. ISO 14577-1:2015. *Metallic materials – Instrumented indentation test for hardness and materials parameters – Part 1: Test method*. ISO, 2015. 46 p.
17. GOST R 8.748–2011. *Metallic materials – Instrumented indentation test for hardness and materials parameters – Part 1: Test method*. Moscow, Standartinform Publ., 2011. 28 p. (In Russian).
18. GB/T 21838.1-2019. *Metallic materials – Instrumented indentation test for hardness and materials parameters – Part 1: Test method*. State Administration for Market Regulation, National Standardization Administration. China, 2019. 40 p.
19. Wu S.-J., Chin P.-C., Liu H. Measurement of elastic properties of brittle materials by ultrasonic and indentation methods. *Applied Sciences*, 2019, vol. 9 (10), p. 2067. DOI: 10.3390/app9102067.
20. Broitman E. Indentation hardness measurements at macro-, micro-, and nanoscale: A critical overview. *Tribology Letters*, 2017, vol. 65 (1), art. 23. DOI: 10.1007/s11249-016-0805-5.
21. Zolotarevskii V.S. *Mekhanicheskie svoistva metallov* [Mechanical properties of metals]. 3rd ed. Moscow, MISIS Publ., 1998. 400 p.
22. Fougere G.E., Riester L., Ferber M., Weertman J.R., Siegel R.W. Young's modulus of nanocrystalline Fe measured by nanoindentation. *Materials Science and Engineering: A*, 1995, vol. 204(1–2), pp. 1–6. DOI: 10.1016/0921-5093(95)09927-1.
23. Noskova N.I., Mulyukov R.R. *Submikrokristallicheskie i nanokristallicheskie metally i splavy* [Submicrocrystalline and nanocrystalline metals and alloys]. Ekaterinburg, UrO RAN Publ., 2003. 279 p.
24. Lutfullin R.Ya., Trofimov E.A., Kashaev R.M., Sitdikov V.D., Lutfullin T.R. Young's modulus of titanium alloy VT6S and its structural sensitivity. *Letters on Materials*, 2017, vol. 7 (1), pp. 12–16. DOI: 10.22226/2410-3535-2017-1-12-16.
25. Sumner D.R., Turner T.M., Igloria R., Urban R.M., Galante J.O. Functional adaptation and ingrowth of bone vary as a function of hip implant stiffness. *Journal of Biomechanics*, 1998, vol. 31 (10), pp. 909–917. DOI: 10.1016/S0021-9290(98)00096-7.



26. Zhang L., Chen L. A review on biomedical titanium alloys: Recent progress and prospect. *Advanced Engineering Materials*, 2019, vol. 21 (4), p. 1801215. DOI: 10.1002/adem.201801215.
27. Wang X., Gong X., Chou K. Scanning speed effect on mechanical properties of Ti-6Al-4V alloy processed by electron beam additive manufacturing. *Procedia Manufacturing*, 2015, vol. 1, pp. 287–295. DOI: 10.1016/j.promfg.2015.09.026.
28. Savchenko N.L., Vorontsov A.V., Utyaganova V.R., Eliseev A.A., Rubtsov V.E., Kolubaev E.A. Osobennosti strukturno-fazovogo sostoyaniya splava Ti-6Al-4V pri formirovani izdelii s ispol'zovaniem elektronno-luchevoi provolochnoi additivnoi tekhnologii [Features of the structural-phase state of the alloy Ti-6Al-4V in the formation of products using wire-feed electron beam additive manufacturing]. *Obrabotka metallov (tekhnologiya, oborudovanie, instrumenty) = Metal Working and Material Science*, 2018, vol. 20, no. 4, pp. 60–71. DOI: 10.17212/1994-6309-2018-20.4-60-71.
29. Osipovich K., Kalashnikov K., Chumaevskii A., Gurianov D., Kalashnikova T., Vorontsov A., Zykova A., Utyaganova V., Panfilov A., Nikolaeva A., Dobrovolskii A., Rubtsov V., Kolubaev E. Wire-feed electron beam additive manufacturing: A review. *Metals*, 2023, vol. 13 (2), p. 279. DOI: 10.3390/met13020279.
30. Pushilina N.S., Klimenov V.A., Cherepanov R.O., Kashkarov E.B., Fedorov V.V., Syrtanov M.S., Lider A.M., Laptev R.S. Beam current effect on microstructure and properties of electron-beam-melted Ti-6Al-4V alloy. *Journal of Materials Engineering and Performance*, 2019, vol. 28 (10), pp. 6165–6173. DOI: 10.1007/s11665-019-04344-0.
31. Okulov I.V., Geslin P.-A., Soldatov I.V., Ovri H., Joo S.-H., Kato H. Anomalously low modulus of the interpenetrating-phase composite of Fe and Mg obtained by liquid metal dealloying. *Scripta Materialia*, 2019, vol. 163, pp. 133–136. DOI: 10.1016/j.scriptamat.2019.01.017.
32. Belosludtsev T.N., Kotolomov A.Yu., Nastich S.Yu., Lopatkin V.A., Shipilov A.V., Kuranov A.Ye., Yaremenko O.B. Opredelenie mekhanicheskikh svoystv metalla kol'tsevykh svarnykh soedinenii i osnovnogo metalla trub metodom instrumental'nogo indentirovaniya [Determining mechanical properties of circular welded joint metal and pipe base metal using the instrumented indentation method]. *Gazovaya promyshlennost' = GAS Industry of Russia*, 2021, no. S3 (823), pp. 26–36. (In Russian).
33. Yaremenko O.B., Kuranov A.E., Vasil'tsov S.Yu. [Instrumental indentation as a non-destructive method for evaluating the mechanical characteristics of structural materials]. *Zhivuchest' i konstruktsionnoe materialovedenie (ZhivKoM – 2020) [Survivability and Structural Materials Science (SSMS-2020)]*. Moscow, 2020, pp. 274–278. (In Russian).
34. Klimenov V., Kolubaev E., Klopotov A., Chumaevskii A., Ustinov A., Strelkova I., Rubtsov V., Gurianov D., Han Z., Nikonov S., Batranin A., Khimich M. Influence of the coarse grain structure of a titanium alloy Ti-4Al-3V formed by wire-feed electron beam additive manufacturing on strain inhomogeneities and fracture. *Materials*, 2023, vol. 16 (11), p. 3901. DOI: 10.3390/ma16113901.
35. ASTM E494-15. *Standard practice for measuring ultrasonic velocity in materials*. ASTM International, 2015.
36. Lee J.-S., Jang J., Lee B.-W., Choi Y., Lee S.G., Kwon D. An instrumented indentation technique for estimating fracture toughness of ductile materials: A critical indentation energy model based on continuum damage mechanics. *Acta Materialia*, 2006, vol. 54 (4), pp. 1101–1109. DOI: 10.1016/j.actamat.2005.10.033.
37. Rafi H.K., Karthik N.V., Gong H., Starr T.L., Stucker B.E. Microstructures and mechanical properties of Ti-6Al-4V parts fabricated by selective laser melting and electron beam melting. *Journal of Materials Engineering and Performance*, 2013, vol. 22 (12), pp. 3872–3883. DOI: 10.1007/s11665-013-0658-0.
38. Collins P.C., Brice D.A., Samimi P., Ghamarian I., Fraser H.L. Microstructural control of additively manufactured metallic materials. *Annual Review of Materials Research*, 2016, vol. 46 (1), pp. 63–91. DOI: 10.1146/annurev-matsci-070115-031816.
39. Liu S., Shin Y.C. Additive manufacturing of Ti-6Al-4V alloy: A review. *Materials & Design*, 2019, vol. 164, p. 107552. DOI: 10.1016/j.matdes.2018.107552.
40. Ho W.F., Ju C.P., Chern Lin J.H. Structure and properties of cast binary Ti–Mo alloys. *Biomaterials*, 1999, vol. 20 (22), pp. 2115–2122. DOI: 10.1016/S0142-9612(99)00114-3.
41. Klimenov V.A., Fedorov V.V., Slobodyan M.S., Pushilina N.S., Strelkova I.L., Klopotov A.A., Batranin A.V. Microstructure and compressive behavior of Ti-6Al-4V alloy built by electron beam free-form fabrication. *Journal of Materials Engineering and Performance*, 2020, vol. 29 (11), pp. 7710–7721. DOI: 10.1007/s11665-020-05223-9.
42. Zardiackas L.D., Mitchell D.W., Disegi J.A. Characterization of Ti-15Mo beta titanium alloy for orthopaedic implant applications. *Medical Applications of Titanium and Its Alloys: The Material and Biological Issues*. ASTM, 1996, pp. 60–75. DOI: 10.1520/stp16070s.



43. Majumdar P., Singh S.B., Chakraborty M. Elastic modulus of biomedical titanium alloys by nano-indentation and ultrasonic techniques – A comparative study. *Materials Science and Engineering: A*, 2008, vol. 489 (1–2), pp. 419–425. DOI: 10.1016/j.msea.2007.12.029.
44. Rakhshadt A.G., Brostrem V.A., eds. *Spravochnik metallista*. V 5 t. T. 2 [Handbook of metalworker. In 5 vols. Vol. 2]. 3rd ed., rev. Moscow, Mashinostroenie Publ., 1976. 720 p.
45. Simonelli M., Tse Y.Y., Tuck C. Effect of the build orientation on the mechanical properties and fracture modes of SLM Ti-6Al-4V. *Materials Science and Engineering: A*, 2014, vol. 616, pp. 1–11. DOI: 10.1016/j.msea.2014.07.086.
46. Keist J.S., Palmer T.A. Role of geometry on properties of additively manufactured Ti-6Al-4V structures fabricated using laser based directed energy deposition. *Materials & Design*, 2016, vol. 106, pp. 482–494. DOI: 10.1016/j.matdes.2016.05.045.
47. Shunmugavel M., Polishetty A., Littlefair G. Microstructure and mechanical properties of wrought and additive manufactured Ti-6Al-4V cylindrical bars. *Procedia Technology*, 2015, vol. 20, pp. 231–236. DOI: 10.1016/j.protcy.2015.07.037.
48. Da Rocha S.S., Adabo G.L., Henriques G.E.P., Nóbilo M.A.d.A. Vickers hardness of cast commercially pure titanium and Ti-6Al-4V alloy submitted to heat treatments. *Brazilian Dental Journal*, 2006, vol. 17 (2), pp. 126–129. DOI: 10.1590/s0103-64402006000200008.
49. Brandl E., Baufeld B., Leyens C., Gault R. Additive manufactured Ti-6Al-4V using welding wire: Comparison of laser and arc beam deposition and evaluation with respect to aerospace material specifications. *Physics Procedia*, 2010, vol. 5, pp. 595–606. DOI: 10.1016/j.phpro.2010.08.087.
50. Galarraga H., Lados D.A., Dehoff R.R., Kirka M.M., Nandwana P. Effects of the microstructure and porosity on properties of Ti-6Al-4V ELI alloy fabricated by electron beam melting (EBM). *Additive Manufacturing*, 2016, vol. 10, pp. 47–57. DOI: 10.1016/j.addma.2016.02.003.

Conflicts of Interest

The authors declare no conflict of interest.

© 2023 The Authors. Published by Novosibirsk State Technical University. This is an open access article under the CC BY license (<http://creativecommons.org/licenses/by/4.0>).

